ACADEMIC PRESS

Available online at www.sciencedirect.com
SCIENCE DIRECT®

Journal of Catalysis 219 (2003) 8–16

JOURNAL OF CATALYSIS

www.elsevier.com/locate/jcat

# Aliovalent-substituted chromium-based catalysts for the hydrofluorination of tetrachloroethylene

Y. Zhu,[1] K. Fiedler, St. Rüdiger, and E. Kemnitz *

*Institute of Chemistry, Humboldt University Berlin, Brook-Taylor-Str. 2, 12489 Berlin, Germany*

Received 14 January 2003; revised 4 April 2003; accepted 4 April 2003

**Abstract**

New aliovalent-doped chromium oxide and fluoride catalysts have been prepared by coprecipitation techniques to obtain solid solutions. The catalysts have been characterized by, e.g., X-ray, BET, and pyridine adsorption analysis, and tested for their catalytic activity in the gas-phase reaction of $C_2Cl_4$ with HF. The latter reaction involves several consecutive steps and produces the expected $C_2HCl_xF_y$ ($x + y = 5$) compounds, but also some perhalogenated compounds the formation of which needs further explanation. Reaction data obtained with a $(Cr,Mg)(F,OH)_x$ catalyst were used to calculate reaction rates and activation energies of all the consecutive steps which could be successfully used to predict the reaction outcomes under varying experimental conditions.


*Keywords:* Aliovalent-doped catalyst; Chromium oxide; Chromium fluoride; Hydrofluorination; Tetrachloroethylene; Mathematical modeling

## 1. Introduction

A wide range of solid catalysts is in use for heterogeneously catalyzed fluorination reactions. Oxides, oxofluorides, and fluorides of aluminium and chromium are suitable fluorination catalysts [1,2]. The catalyzed halogen exchange reactions involve Cl/F exchange [Eq. (1)], hydrofluorination [Eq. (2)], dismutation [Eq. (3)], and isomerization [Eq. (4)],

$$\text{R–Cl} + \text{HF} \rightarrow \text{R–F} + \text{HCl}, \tag{1}$$

$$\text{X}_2\text{C=CX}_2 + \text{HF} \rightarrow \text{X}_2\text{HC–CFX}_2 \quad (\text{X} = \text{halogen}), \tag{2}$$

$$2\text{CCl}_2\text{F–CClF}_2 \rightarrow \text{CCl}_3\text{–CClF}_2 + \text{CCl}_2\text{F–CF}_3, \tag{3}$$

$$\text{CHF}_2\text{–CHF}_2 \rightarrow \text{CH}_2\text{F–CF}_3. \tag{4}$$

Dehydrohalogenation reactions, which can be regarded as the back reaction of (2), might principally also be considered. Usually, all these processes start with the respective oxides as catalyst, although it has been proven that the oxide materials become at least partially fluorinated by the haloalkane in the course of the activation [3–7]. It is furthermore reported, that partial substitution of the metal cation affects the catalytic properties. Hence, $\gamma$-alumina has been modified with alkali [8,9] and alkaline earth [10] metals, and with d-elements [11–15]. Chromia, modified with zinc, nickel, or magnesium by means of an impregnation technique, has been investigated recently [16]. Zinc is described to generate enhancedly catalytic surface sites, although the bulk structure of the chromia host is not affected. The other metals like nickel and magnesium are reported not to exhibit this special effect, which is in agreement with reports by other authors [17,18]. Since most of these catalysts were prepared by impregnation techniques, it is very difficult to draw decisive conclusions about the real catalytic phases formed at the surface. For a deeper understanding, the formation of solid solutions (e.g., by coprecipitation) as long as it results in homogeneous solid solutions allows a better assignment of the observed effects. However, for some systems solid solutions cannot be formed even by employing coprecipitation methods because this mainly depends on the intrinsic properties of the system itself.

Among the above noted halogen exchange reaction, the transformation of C–Cl bonds into C–F bonds by fluorination of respective chlorinated alkanes is one of the most important industrial reactions because this involves the large-scale production of hydrofluorocarbons (HFCs), which are the replacements of ozone depleting chlorofluorocarbons (CFCs). Compared to CFC production, HFC syn-

* Corresponding author.
*E-mail address:* erhard.kemnitz@chemie.hu-berlin.de (E. Kemnitz).
[1] On leave from Institute of Physical Chemistry, Peking University, 100871 Beijing, PR China.

0021-9517/$ – see front matter 
doi:10.1016/S0021-9517(03)00183-0

thesis is more complicated. One of the reasons for significantly more complicated reaction systems is the instability of hydrogen-containing haloalkanes against ethylene formation by splitting off HX. There are three interesting $C_2$-HFC series: $C_2H_3Y_{3-x}X_x$, $C_2H_2Y_{4-y}X_y$, and $C_2HY_{5-z}X_z$ (Y = Cl, X = F, $x = 0$–3, $y = 0$–4, $z = 0$–5). For the synthesis of $CH_3CF_3$ (HFC-143a) and $CH_2FCF_3$ (HFC-134a), respectively, the mechanistic pathway of these catalytic reactions has been investigated in detail [19,20]. It was shown that, starting with the respective chloroethylenes, the reaction system consists of competitive Cl/F exchange and dehydrohalogenation/hydrohalogenation reactions. Hence, olefin formation is a crucial step in these reactions. However, no comparable investigations of the reaction course in the $C_2HY_{5-z}X_z$ series has been done by now.

Hence, this paper deals with the study of new aliovalent-doped chromium oxide and fluoride catalysts, which are used in the catalytic fluorination reaction of tetrachloroethylene by gaseous HF to obtain derivatives of the $C_2HY_{5-z}X_z$ series. The formation of $C_2Y_{6-z}X_z$ series products was also investigated.

## 2. Experimental

The oxide samples were prepared by adding a 3 M $NH_3 \cdot H_2O$ solution to the aqueous solutions of the corresponding metal nitrates (Cr and V) or chloride (Zr) to a pH value of 8 to 9. After ageing at about 90 °C for 1 h, the precipitants were filtrated and washed with deionized water, dried at 80 °C overnight, and then calcined at 300 °C for 8 h under $N_2$. Before the catalysis tests, oxide samples were fluorinated in situ. The samples (0.5–0.8-mm particles) were first pretreated at 300 °C under $N_2$ for 0.5 h and then fluorinated at 400 °C in gas mixture of 7.0 ml/min HF and 6.3 ml/min $N_2$ for 2 h. All the characterizations were performed on the partially fluorinated samples. The oxide catalysts were designated $CrO_x$ and CrMOY, respectively (M = doping metal, V or Zr; Y = mol% of doping metal).

The $(Cr,V)(F,OH)_x$ and $(Cr,Zr)(F,OH)_x$ fluoride samples were prepared by adding the ethanolic solution of chromium nitrate into 40% HF aqueous solution in which appropriate amounts of $ZrO(NO_3)_2 \cdot xH_2O$ or $V_2O_3$ were predissolved. After stirring for 0.5 h, the precipitants were filtrated and washed with a small amount of deionized water and ethanol, dried at room temperature, and then calcinated at 420 °C (2 °C/min from room temperature to 420 °C) for 2 h in $N_2$ under a self-generated atmosphere. The $(Cr,Mg)(F,OH)_x$ fluoride samples were prepared by adding the ethanolic solution of chromium and magnesium nitrates into 40% HF aqueous solution as described previously [21]. Before catalysis experiments were run, all samples (0.5- to 0.8-mm particles) were first pretreated in situ at 300 °C under $N_2$ for 0.5 h and then fluorinated at 400 °C in a gas mixture of 7.0 ml/min HF and 6.3 ml/min $N_2$ for 2 h. The fluoride catalysts were designated $(Cr,M)(F,OH)_x/Y$ (M = doping metal; Y = mol% of doping metal).

X-ray powder diffraction characterization was carried on XRD 7 Seiffert-FPM with Cu-$K_\alpha$ radiation. BET surface area and desorption pore volume distribution were measured on a Micrometrics ASAP 2000 analyzer using $N_2$ as the adsorbent. Fluoride content was determined as previously described [22]. The characteristic data for related samples are summarised in Tables 1 and 2. The number in the sample name refers to the molar percent of the doping metal.

FT-IR photoacoustic pyridine adsorption spectroscopy (pas) was done as follows. About 80 mg sample was pretreated at 150 °C under a nitrogen flow of 35 ml/min for 15 min, and then 60 µl pyridine was injected to the sample tube. The sample was flushed with nitrogen for another 15 min to remove physisorbed pyridine. A spectrum of the sample was taken at room temperature using an MTEC cell and FT-IR System 2000 (Perkin-Elmer). A spectrum of the sample without pyridine absorption was also taken as background.

Temperature-programmed desorption of ammonia ($NH_3$-TPD) was employed for the determination of the strength distribution of acid sites. About 200 mg sample (0.3–0.5-mm diameter fraction) was pretreated under nitrogen (35 ml/min) at 400 °C for 1 h, then cooled to 120 °C, and then exposed to $NH_3$. The physisorbed ammonia was removed over 1 h at 120 °C. After cooling to 80 °C, the TPD program (10 °C/min, up to 460 °C, keeping 30 min) was started. The desorption of ammonia was monitored by continuously running IR spectroscopy (FT-IR System 2000, Perkin-Elmer).

Table 1
Composition, specific surface area, and intensity of photoacoustic pyridine adsorption (pas) band at 1452 $cm^{-1}$ for fluorinated oxide catalysts

| Catalyst | Composition | F content (%) | Surface area ($m^2/g$) | Intensity of pas band |
|---|---|---|---|---|
| CrOx | $CrO_{1.04}F_{0.92}$ | 20.38 | 152 | 9.4 |
| CrVO5 | $Cr_{0.95}V_{0.05}O_{1.11}F_{0.78}$ | 17.58 | 231 | 11.7 |
| CrVO10 | $Cr_{0.90}V_{0.10}O_{1.13}F_{0.75}$ | 16.94 | 177 | 9.0 |
| CrVO15 | $Cr_{0.85}V_{0.15}O_{1.18}F_{0.65}$ | 14.85 | 171 | 10.5 |
| CrVO30 | $Cr_{0.70}V_{0.30}O_{1.14}F_{0.72}$ | 16.37 | 126 | 9.7 |
| CrZrO5 | $Cr_{0.95}Zr_{0.05}O_{1.19}F_{0.67}$ | 14.92 | 137 | 10.1 |
| CrZrO10 | $Cr_{0.90}Zr_{0.10}O_{1.12}F_{0.86}$ | 19.79 | 127 | 14.2 |
| CrZrO20 | $Cr_{0.80}Zr_{0.20}O_{1.00}F_{1.20}$ | 23.17 | 107 | 18.0 |
| CrZrO30 | $Cr_{0.70}Zr_{0.30}O_{0.95}F_{1.41}$ | 25.35 | 77 | 17.5 |

Table 2
Composition, specific surface area, and intensity of photoacoustic pyridine adsorption (pas) band at 1452 $cm^{-1}$ for fluoride catalysts

| Catalyst | F content (%) | XRD | Surface area ($m^2/g$) | Intensity of pas band |
|---|---|---|---|---|
| $Cr(F,OH)_x$ | 41.57 | Amorphous | 8.0 | 2.9 |
| $(Cr,V)(F,OH)_x/5$ | 39.99 | Amorphous | 5.5 | 1.3 |
| $(Cr,V)(F,OH)_x/10$ | 40.28 | Amorphous | 5.6 | 1.5 |
| $(Cr,V)(F,OH)_x/26$ | 41.35 | Amorphous | 7.0 | 1.9 |
| $(Cr,V)(F,OH)_x/46$ | 44.85 | Amorphous | 8.1 | – |
| $(Cr,Zr)(F,OH)_x/5$ | 39.23 | Amorphous | 4.1 | 1.1 |
| $(Cr,Zr)(F,OH)_x/15$ | 36.53 | Amorphous | 5.6 | 2.1 |
| $(Cr,Zr)(F,OH)_x/30$ | 43.67 | Unknown | 3.1 | 1.8 |
| $(Cr,Mg)(F,OH)_x/60$ | 52.21 | $MgF_2$ | 106 | 7.9 |
| $(Cr,Mg)(F,OH)_x/80$ | 54.19 | $MgF_2$ | 106 | 12.6 |

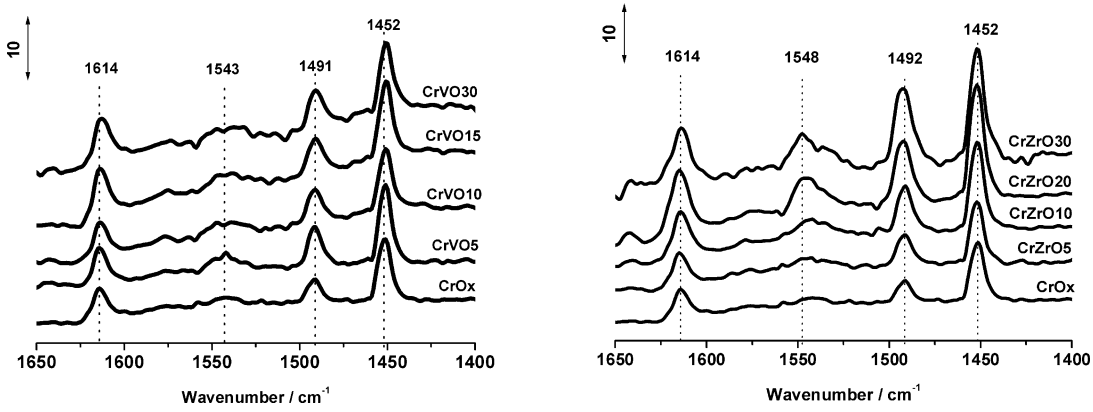


Fig. 1. FT-IR photoacoustic pyridine adsorption profiles of chromium oxide catalysts with different dopants.

Catalytic tests were carried out with the in situ pretreated samples using a flow reactor (nickel tube). The catalytic reaction was investigated using a gas mixture of 1.2 ml/min $C_2Cl_4$ + 7.0 ml/min HF + 6.3 ml/min $N_2$. A contact time of 10 s was used for the regular test at different temperatures. The gaseous product mixture was analyzed on-line, after passing a solid NaF HF scrubber, by GC-FID with a 10% SE 30 Chromsorb column. In addition, GC-MS and 19-F NMR were used off-line for identification of the by-products. For that, samples were collected by passing the HF-free effluent through an ice-cooled $CHCl_3$/NaF slurry. The solution obtained was subjected to GC, GC-MS (Shimadzu QP 5000, PONA 50 m capillary), and to $^{19}F$ NMR (BRUKER AX 300, $CCl_3F$ extern).

## 3. Results and discussion

### 3.1. Partially fluorinated oxide catalysts

#### 3.1.1. General physicochemical properties

X-ray powder diffraction showed that all the samples were in an amorphous state. As can be seen in Table 1, modification of chromium oxide with vanadium and zirconium resulted in substantial changes in the specific surface areas. Samples doped with vanadium had higher specific surface areas than pure chromium oxide, while the addition of zirconium decreased the surface area. However, compared to the fluoride catalysts (Table 2), all chromium oxide-based catalysts had quite high surface areas and high intensities in the FT-IR photoacoustic spectra of pyridine adsorption. As shown in Fig. 1, vanadium-doped catalysts had more or less similar spectra of photoacoustic pyridine adsorption to that of the undoped chromium oxide, while the spectra of zirconium-doped catalysts showed much higher intensity at 1452 $cm^{-1}$ which is characteristic of Lewis acid sites and 1548 $cm^{-1}$ which belongs to the Bronsted acid sites. However, it is worth noting that pas intensities can be regarded semiquantitatively at its best, despite giving pas intensities in Tables 1 and 2.

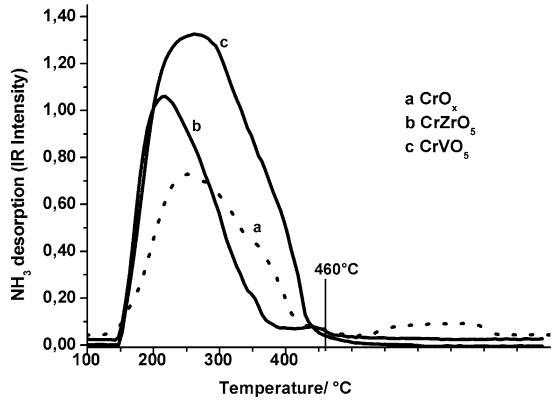


Fig. 2. $NH_3$-TPD profiles of selected oxide catalysts.

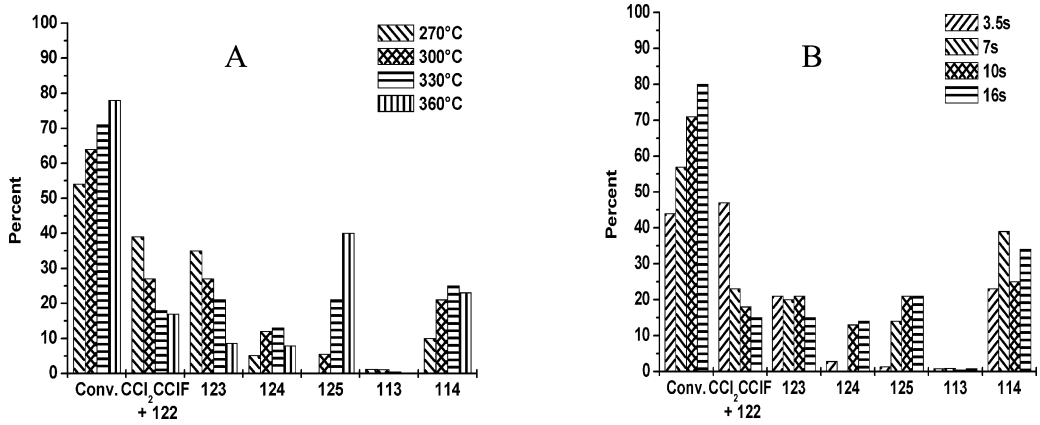


Fig. 3. Catalytic property of fluorinated chromium oxide CrOx. (A) Effect of reaction temperatures at a contact time of 10 s. (B) Effect of contact time at 330 °C.

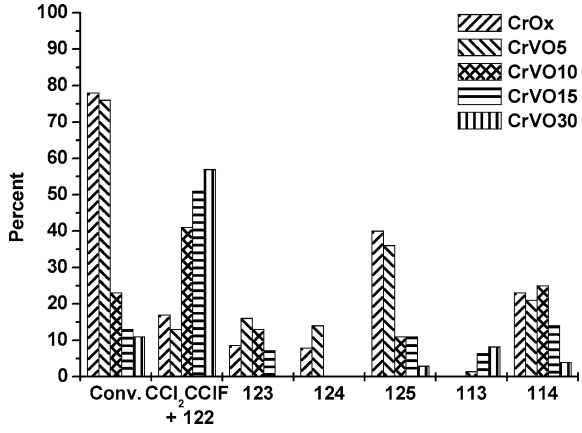


Fig. 4. Conversion of $C_2Cl_4$ and its selectivity to various HCFCs on fluorinated CrVOY (Y = 0, 5, 10, 15, and 30) catalysts.

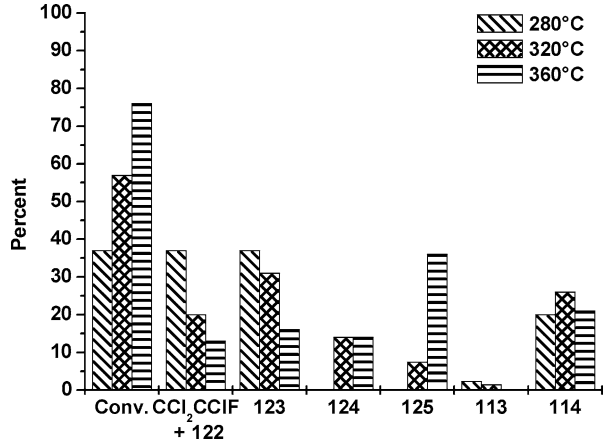


Fig. 5. Conversion of $C_2Cl_4$ and its selectivity to various HCFCs on CrVO5 at different temperatures.

For selected samples, $NH_3$-TPD measurements were further performed to characterize the strength distribution of the acid sites (Fig. 2). Vanadium-doped sample CrVO5 showed similar distribution to CrOx, whereas addition of the same amount of zirconium decreased the average strength of the acid sites.

### *3.1.2. Catalytic activities*

The catalytic test was first carried out on pure chromium oxide under different reaction conditions. Fig. 3 shows the effect of reaction temperature at a contact time of 10 s and the effect of contact time at a reaction temperature of 330 °C on the conversion of $C_2Cl_4$ and the product distribution. It can be seen that at 360 °C the conversion of $C_2Cl_4$ was highest reaching 78%, yielding mostly (40%) HFC-125, the highest fluorinated HFC, besides some HCFC-124 and quite a lot CFC-114. With reduced reaction temperature, the conversion decreases, and the selectivity to HFC-125 decreases significantly, too, while less fluorinated compound became predominant. Besides reaction temperature, change of the contact time also had an effect on both catalytic activity and selectivity. Longer contact times resulted in higher conversion of $C_2Cl_4$ and increased formation of higher fluorinated compounds; however, it was evident that reaction temperature had a more profound effect.

Fig. 4 shows the results of the catalytic tests of vanadium-doped samples at a reaction temperature of 360 °C. It can be seen that increase in vanadium content caused a dramatic decrease in the catalytic activity and likewise in the selectivity toward HFC-125, but an increase in the formation of lower fluorinated compounds. Only the sample with 5% vanadium, CrVO5, exhibited conversion and selectivity similar to those of pure chromium oxide, though all vanadium-doped samples had high surface areas and similar acidities as characterized by photoacoustic pyridine adsorption. This means that the number of the surface acid sites is not the only parameter affecting the catalytic property.

The catalytic behavior of CrVO5 at different temperatures was also investigated at a contact time of 10 s. As shown in Fig. 5, the change in the conversion of $C_2Cl_4$ as well as the selectivity to HFC-125 with reaction temperature was much more significant compared with that of pure chromium oxide, which indicates that the activation energy on CrVO5 is higher than that on CrOx. Under all conditions tested (viz.

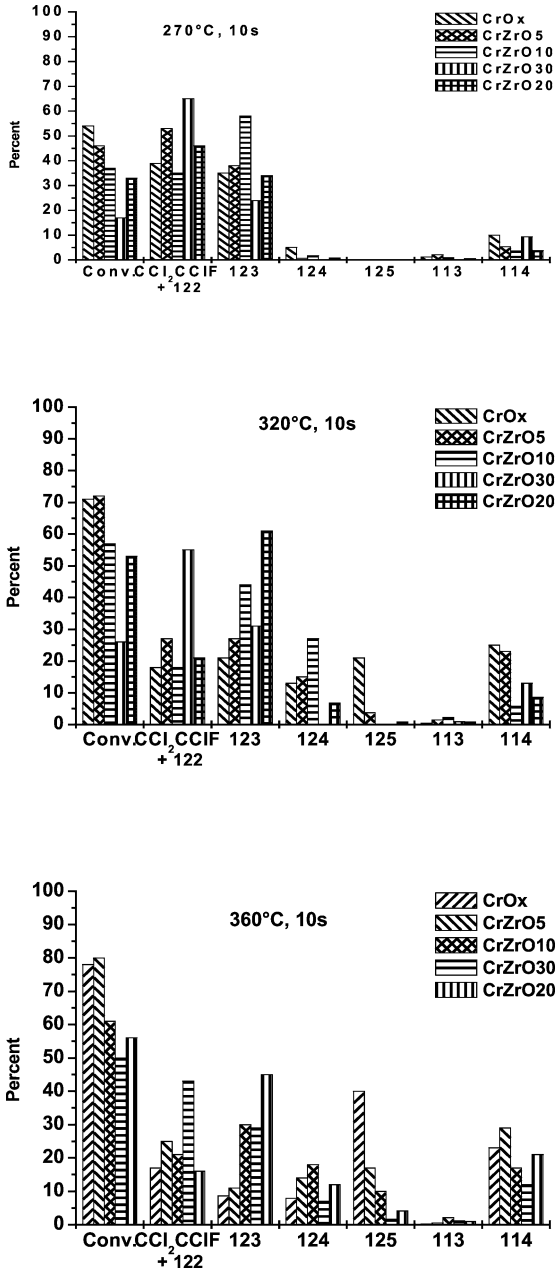


Fig. 6. Conversion of $C_2Cl_4$ and its selectivity to various HCFCs on CrZrOY (Y = 0, 5, 10, 20, and 30) catalysts at different temperatures.

Figs. 4 and 5) there was a substantial formation of fully halogenated CFCs, mostly of CFC-114a.

The catalytic properties of zirconium-doped samples were investigated at three different temperatures (Fig. 6). The catalytic activity decreased with increasing zirconium content, but not so dramatic compared with that of vanadium-doped samples. The conversion decreased from 80 to 50% when zirconium content increased from 5 to 30% though the number of the surface acid sites increased, too. The effect of the reaction temperature on the catalytic activity was similar to those observed with pure chromium oxide and vanadium-doped samples, but the selectivity changed significantly. For example, at a reaction temperature of 360 °C, the selectivity to HFC-125 on CrZrO5 was only 17% compared with 40% on undoped CrOx, even though the conversion of $C_2Cl_4$ was also quite high in the former case. However, these zirconium-doped samples produced much more HCFC-123. Thus the sample with 20% zirconium, CrZrO20, gave 61% selectivity toward HCFC-123, however, with a medium conversion (53%) of $C_2Cl_4$, and it may be a good candidate for the production of HCFC-123. The appreciable selectivity of CrZrO catalyst can be probably attributed to its lower strength of the acid sites as shown in the $NH_3$-TPD profiles.

### 3.2. Fluoride catalysts

#### 3.2.1. General physicochemical properties

The composition, surface area, morphology, and Lewis acidity of some fluoride catalysts are given in Table 2. Similar to undoped $Cr(F,OH)_x$, the vanadium- and zirconium-doped catalysts were also in an amorphous state except $(Cr,Zr)(F,OH)_x/30$, and had low surface areas. In contrast, $(Cr,Mg)(F,OH)_x$ samples with high surface area displayed XRD patterns of $MgF_2$ (Fig. 7). However, the diffraction peaks of $(Cr,Mg)(F,OH)_x/60$ and $(Cr,Mg)(F,OH)_x/80$ are much broader than those of pure $MgF_2$, indicating that the crystal size of $MgF_2$ had become much smaller, resulting in a much higher surface area. This point is further supported by the pore-size distribution shown in Fig. 8 on the assumption that the pore size is of the same level as particle size. In Fig. 8, $MgF_2$ shows a narrow peak centred at 400 Å, while $(Cr,Mg)(F,OH)_x/80$ shows also narrow peak but with a much smaller size of 35 Å. In the pore-size distribution profile of $(Cr,Mg)(F,OH)_x/60$, there is a very broad peak between 300 and 1500 Å besides the narrow peak at 35 Å. Referring to the broad peak of $Cr(F,OH)_x$, it can be deduced that there is some isolated amorphous $Cr(F,OH)_x$ phase in the sample of $(Cr,Mg)(F,OH)_x/60$, while in the sample of $(Cr,Mg)(F,OH)_x/80$, the chromium species is either dispersed on the surface of $MgF_2$ particle or incorpo-

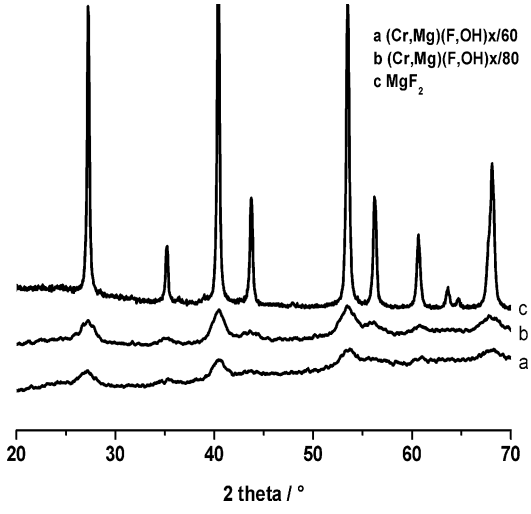


Fig. 7. XRD patterns of $(Cr,Mg)(F,OH)_x$ samples.

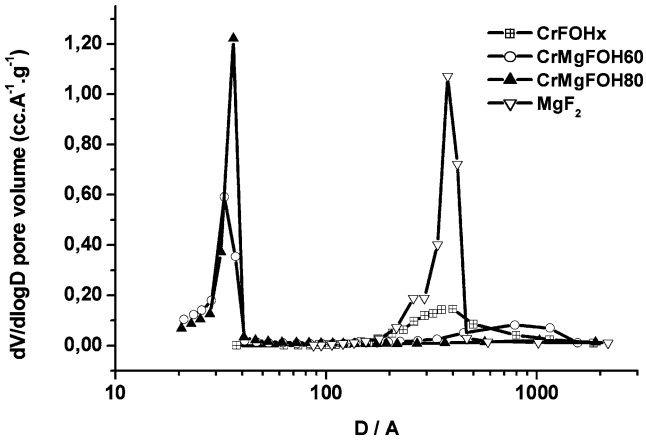


Fig. 8. d$V$/d log $D$ pore volume distribution of (Cr,Mg)(F,OH)$_x$ samples.

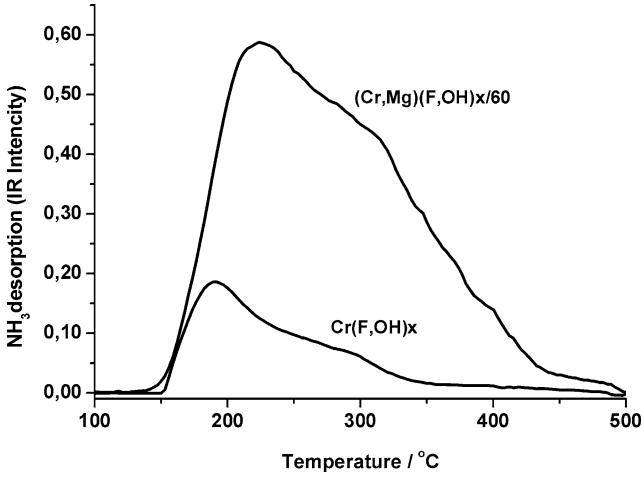


Fig. 9. $NH_3$-TPD profiles of Cr(F,OH)$_x$ and (Cr,Mg)(F,OH)$_x$/60.

rated into the lattice of $MgF_2$ to form a solid solution, but there is no evident shift in the XRD peaks.

As shown in Table 2, V- and Zr-doped chromium fluoride samples had most probably only small amounts of Lewis acid sites on their surface. On the other hand, (Cr,Mg)(F,OH)$_x$/60 and (Cr,Mg)(F,OH)$_x$/80 show higher intensities comparable to that of oxide catalyst in FT-IR photoacoustic spectra of pyridine adsorption. $NH_3$-TPD profiles were also measured for (Cr,Mg)(F,OH)$_x$/60 and Cr(F,OH)$_x$, and they are shown in Fig. 9. Clearly, (Cr,Mg)(F,OH)$_x$/60 has many more acid sites than Cr(F,OH)$_x$, and the strength of the acidity is also enhanced.

### 3.2.2. Catalytic activities

The results of catalytic tests for fluoride catalysts are listed in Table 3. Chromium fluoride as well as V- and Zr-doped catalysts showed relatively low activities because of their low surface areas and fewer acid sites. The main products from these catalysts were the lowest fluorinated HCFC-122 and $CCl_2CClF$, the latter is possibly derived from HCFC-121. Among the higher fluorinated products CFC-113 and CFC-114a were always present; in all experiments the sum of their respective selectivities exceeded the sum of the selectivities of the other minor products. As expected, (Cr,Mg)(F,OH)$_x$/60 and (Cr,Mg)(F,OH)$_x$/80 were quite active, and the main products were higher fluorinated HFC-125 and HCFC-124. And most interestingly, they produced almost no CFC-110 series by-products.

### 3.3. Theoretical calculation

The results of the catalytic measurements indicate that the fluorination of tetrachloroethylene with HF proceeds via a complex system of consecutive and competitive reactions. Besides the expected HCFC-12X series compounds, chlorofluoroethylene with varying fluorine numbers and certain amounts of CFC-11X series (which are also observed in industrial processes) are also formed (see later). Ignoring these products, a simplified reaction pathway can be summarized in Scheme 1. The distribution of the products depends not only on the activity of the catalyst, but also on the reaction conditions. The highest selectivity to a special product can be possibly obtained by modulating the reaction conditions.

Table 3
The results of the catalytic measurement for fluoride catalysts

| Sample | Reaction condition | Conversion (%) | Selectivity (%)[a] | | | | | |
|---|---|---|---|---|---|---|---|---|
| | | | $CCl_2CClF + 122$ | 113 | 123 | 114a | 124 | 125 |
| Cr(F,OH)$_x$ | 360 °C, 10 s | 14 | 58 | 8.9 | 4.5 | 14 | 1.5 | 3.3 |
| (Cr,V)(F,OH)$_x$/5 | 360 °C, 10 s | 7.6 | 53 | 7.2 | 3.2 | 15 | 0 | 5.2 |
| (Cr,V)(F,OH)$_x$/10 | 360 °C, 10 s | 9.1 | 66 | 6.2 | 4.3 | 8.3 | 0 | 3.0 |
| (Cr,V)(F,OH)$_x$/26 | 360 °C, 10 s | 4.6 | 35 | 11 | 0 | 3.7 | 0 | 1.6 |
| (Cr,Zr)(F,OH)$_x$/5 | 360 °C, 10 s | 14 | 47 | 14 | 4.7 | 14 | 0 | 3.2 |
| (Cr,Zr)(F,OH)$_x$/15 | 360 °C, 10 s | 10 | 68 | 2.3 | 9.7 | 15 | 0 | 1.3 |
| (Cr,Zr)(F,OH)$_x$/30 | 360 °C, 10 s | 5.3 | 54 | 1.8 | 7.8 | 12 | 0 | 0 |
| (Cr,Mg)(F,OH)$_x$/60 | 360 °C, 10 s | 78 | 4.0 | 1.0 | 5.9 | 0 | 22 | 67 |
| | 320 °C, 16 s | 69 | 7.0 | 1.0 | 18 | 0 | 40 | 34 |
| | 320 °C, 10 s | 66 | 8.0 | 0.8 | 20 | 0 | 44 | 27 |
| | 320 °C, 4 s | 41 | 17 | 0.8 | 31 | 8.0 | 33 | 11 |
| | 280 °C, 10 s | 36 | 27 | 0.4 | 53 | 0 | 18 | 0.9 |
| (Cr,Mg)(F,OH)$_x$/80 | 360 °C, 10 s | 58 | 10 | 1.7 | 11 | 0 | 18 | 54 |

[a] The rest are 112, 121, $CCl_2CF_2$; traces of $CHClFCClF_2$ are included in 123; traces of 115 are included in 125.

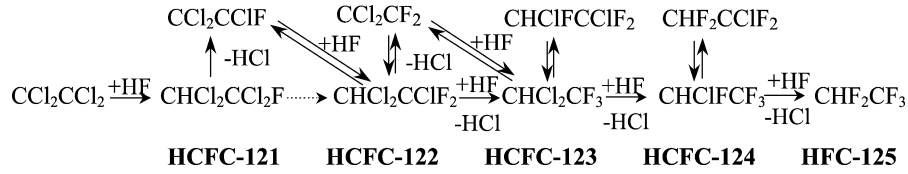


Scheme 1. Reaction pathways of the catalyzed fluorination of tetrachloroethylene with HF (bold arrows, probable path; dotted arrow, less probable path).

In order to estimate the influence of reaction temperature, contact time, and $HF/C_2Cl_4$ ratio on the distribution of the products and the conversion of $C_2Cl_4$, theoretical calculations were performed on $(Cr,Mg)(F,OH)_x/60$ which produces almost no by-products.

A mathematical program was applied which has already been applied and in detail described for the isomerization reaction of $CF_2ClCF_2Cl$ to $CF_3CFCl_2$ that also consists of a system of equilibrium and consecutive reaction steps [23]. Using this program and the experimental data obtained under different conditions (Table 3), one can calculate reaction rates and activation energies of all reaction steps involved, and, consequently, calculate the theoretical product distributions at other reaction conditions. In Fig. 10, the comparison of the results of theoretical calculation with the experimental data is shown. Evidently, the theoretical calculation agrees well with the experimental data. From the theoretical calculation, it can be seen that at 320 °C and an $HF/C_2Cl_4$ ratio of 6:1, short contact time ($< 6$ s) favors the formation of HFC-123, medium contact time (6–16 s) results mainly in HFC-124, and with contact times longer than 16 s, HFC-125 becomes the dominant product. The calculation shows that at constant $HF/C_2Cl_4$ ratio, an increase in the reaction temperature can be compensated by decreased contact time to get similar product distributions. In addition, the influence of the $HF/C_2Cl_4$ ratio on product distribution was also calculated (Fig. 11). Interestingly, HFC-125 can become the major product even at a $HF/C_2Cl_4$ ratio of 4:1, i.e., with less than the stoichiometric amount to form HFC-125, provided the contact time is long enough. And naturally, increase in the $HF/C_2Cl_4$ ratio will greatly decrease the contact time needed to get similar results. However, the influence of the reaction temperature seems more significant than that of the contact time. At 320 °C and $HF/C_2Cl_4$ ratio of 10:1, HFC-125 becomes the main product when the contact time exceeds 8.5 s. But at the lower $HF/C_2Cl_4$ ratio of 6:1 and a higher reaction temperature of 360 °C, HFC-125 becomes the main product at contact times of more than 4.5 s (Fig. 10). This means that the lowest contact time to get HFC-125 is significantly decreased at the higher temperature. According to the results of the theoretical calculations, it is possible to choose suitable reaction conditions to get a specific target product.

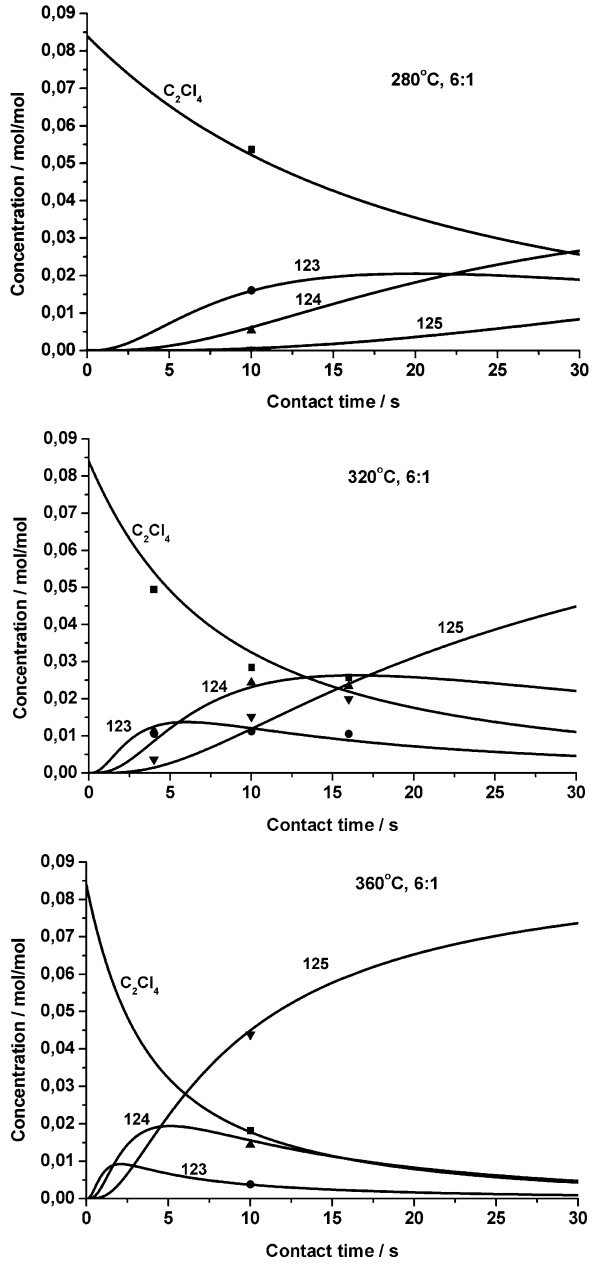


Fig. 10. Comparison of the results of theoretical calculation (line) with the experimental data (symbol).

### 3.4. Formation of CFC-110 series products

Under all reaction conditions tested, different amounts of fully halogenated compounds, i.e., of the CFC-11X-series, were formed in addition to the aimed HCFC-$C_2HY_{5-z}X_z$-series compounds. The formation of, e.g., CFC-114a, and of CFC-113 and CFC-114, which have been confirmed both by $^{19}F$ NMR [24,25] and by GC in comparison with authentic samples, cannot be explained on the basis of con-

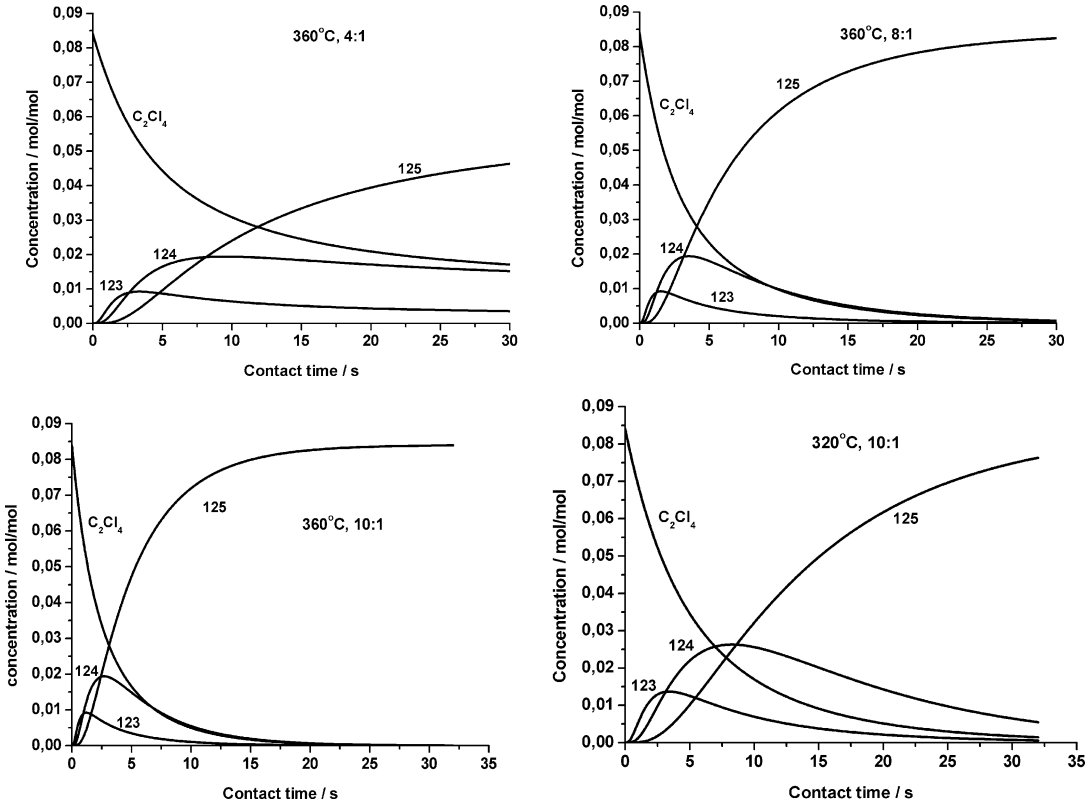


Fig. 11. Results of the theoretical calculation of the products distribution under different conditions.

secutive addition and elimination reactions as exemplified in Scheme 1. Speaking in terms of reaction types, an oxidation reaction had to take place. Whereas the presence of oxygen could be excluded, there is a small possibility, though a very unlikely one, that species with higher oxidation states in the chromium catalyst act as oxidative agents. To exclude this, an experiment was performed under identical conditions but with pure $MgF_2$ as catalyst. The $^{19}F$ NMR spectrum of the effluent is shown in Fig. 12, and the assignment of the spectrum is given in Table 4. As can be seen from Fig. 12 and Table 4, even with an $MgF_2$ catalyst totally halogenated CFCs have been formed in course of the reaction of $C_2Cl_4$ with HF. A quantitative evaluation of the NMR spectrum (Table 4), based on peak integration and subsequent normalization according to the numbers of F atoms in the respective molecules, revealed that the totally halogenated compounds amount to about 33.5% of the mixture. This figure is in good agreement with the GC data. The results with $MgF_2$ indicate that any oxidative action of the catalyst can be excluded as cause of CFC formation. Disproportionation is another possible way of CFC formation. However, starting from HCFC–$C_2HY_{5-z}X_z$-series molecules, for each CFC molecule formed one molecule of the $C_2H_2X_zY_{4-z}$ series must be formed, too, as exemplified schematically in Eq. (5).

$$2C_2HX_xY_{5-x} \rightarrow C_2X_yY_{6-y} + C_2H_2X_zY_{4-z} \quad (\mathrm{X},\ \mathrm{Y} = \mathrm{Cl},\ \mathrm{F};\ x = 0\text{–}5;\ y = 0\text{–}6;\ z = 0\text{–}4). \qquad (5)$$

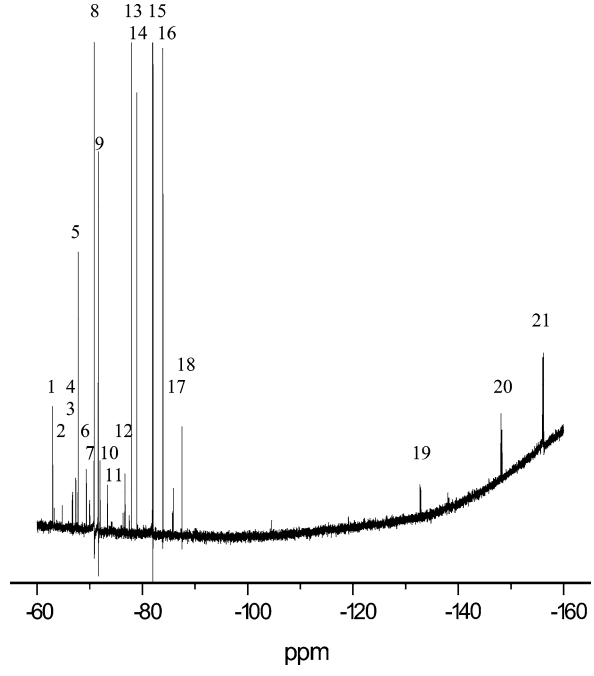


Fig. 12. $^{19}F$ NMR spectrum of a product mixture from the reaction of $C_2Cl_4$ with HF over $MgF_2$.

A further reaction pathway yielding CFCs starts from the primary product, $CHCl_2CCl_2F$, which might undergo dechlorination whereby the chlorine formed should react with, e.g., $C_2Cl_4$ giving $C_2Cl_6$ as starting compound

Table 4
Analysis of a product mixture obtained with $MgF_2$ catalyst by its $^{19}F$ NMR data

| Compound | Peak No. in Fig. 12 | Peak area | Area divided by No. of F atoms | Relative concentration (%) |
|---|---|---|---|---|
| F111 | 1 | 2.46 | 2.46 | 7.3 |
| F112a | 2 | 0.3 | 0.15 | 0.4 |
| F113 | 5 + 10 | 6.23 + 2.93 | 3.05 | 9.1 |
| F114 | 8 | 12.91 | 3.23 | 9.6 |
| F114a | 12 + 16 | 2.18 + 7.38 | 2.39 | 7.1 |
| F123a | 3 + 4 + 6 +7 + 20 | 1.24 + 2.01 + 1.81 +1.2 + 2.53 | 2.93 | 8.7 |
| F123 | 13 | 18.37 | 6.12 | 18.2 |
| F124a | 11 + 19 | 1.61 + 1.71 | 0.83 | 2.5 |
| F124 | 15 + 21 | 24.61 + 5.57 | 7.55 | 22.4 |
| $CCl_2CClF$ | 14 | 4.52 | 4.52 | 13.4 |
| $CCl_2CF_2$ | 18 | 0.94 | 0.47 | 1.4 |
| Unknown | 9 + 17 | 8.43 + 1.23 | – | – |

113 and 114 have also been confirmed by GC in comparison with authentic samples.

for CFCs. However, the primary dechlorination product, ClHC=CClF, will most probably react with the HF giving $CH_2CClF_2$ in quantities equivalent to the amounts of CFC detected.

Surprisingly, such compounds of lower halogen content could not be detected in the product mixture, and the "unknown" peaks in Table 4 account for only 8.7% of the total peak areas in the 19-F NMR spectrum of the mixture. Thus, there is so far no experimental evidence on hand to discriminate between the discussed mechanisms for the observed formation of perhalogenated compounds.

## 4. Conclusions

1. Fluorination of $C_2Cl_4$ with HF involves several consecutive reactions and produces CFC-120 series compounds and chloro-fluoro-ethylenes with different fluorine numbers, and, surprisingly, some perhalogenated compounds, too. The formation of the latter could not be fully elucidated. Higher reaction temperature, longer contact time, and higher $HF/C_2Cl_4$ ratio favor higher fluorinated products.

2. All the chromium oxide-based catalysts possess quite high surface areas and high intensities in the FT-IR photoacoustic spectra of pyridine adsorption. However, only the samples with 5% dopant show similar conversion of $C_2Cl_4$ comparable with that of pure chromium oxide. And it is worth noting that Cr–Zr–O samples show much reduced selectivity to HFC-125 but quite high selectivity to CFC-123. This different selectivity can be probably attributed to the lower strength of the acid sites.

3. Chromium hydroxofluoride as well as V and Zr-doped samples show relatively low surface areas and low catalytic activities whereas $(Cr,Mg)(F,OH)_x$ samples with high surface areas show very high activities and produce almost no by-products.

## References

[1] E. Kemnitz, J.M. Winfield, in: T. Nakajima, A. Tressaud, B. Žemva (Eds.), Advanced Inorganic Fluorides: Synthesis, Characterization and Applications, Elsevier Science, 2000, p. 367.
[2] E. Kemnitz, D.-H. Menz, Progr. Solid State Chem. 26 (1998) 97.
[3] L. Kolditz, V. Nitzsche, G. Heller, R. Stoesser, Z. Anorg. Allg. Chem. 476 (1981) 23.
[4] S. Okazaki, H. Eriguchi, Chem. Lett. (1980) 891.
[5] D. Bechadergue, M. Blanchard, P. Canesson, in: M. Guisnet, et al. (Eds.), Heterogeneous Catalysis and Fine Chemicals, Elsevier, Amsterdam, 1980, p. 257.
[6] A. Hess, E. Kemnitz, J. Catal. 148 (1994) 270.
[7] E. Kemnitz, A. Hess, J. Prakt. Chem. 334 (1992) 591.
[8] P. Berteau, B. Delmon, Catal. Today 57 (1989) 121.
[9] P. Berteau, M.A. Kellens, B. Delmon, J. Chem. Soc., Faraday Trans. 87 (1991) 1425.
[10] J. Schurch, N.W. Cant, D.L. Trimm, Appl. Catal. A 101 (1993) 105.
[11] W. Kania, K. Jurczyk, Appl. Catal. A 61 (1990) 27.
[12] H. Hamada, Y. Kinataichi, M. Sasaki, T. Ito, Appl. Catal. A 75 (1991) 1.
[13] C. Morterra, H. Magnaccia, L. Cerrato, G. del Bavero, K. Fillipi, G. Folonari, J. Chem. Soc., Faraday Trans. 88 (1992) 135.
[14] G. Wend, C.D. Meinecke, W. Schmitz, Appl. Catal. 45 (1988) 209.
[15] W. Kania, K. Jurczyk, Appl. Catal. 56 (1989) 253.
[16] D.W. Bonniface, J.R. Fryer, P. Landon, J.D. Scott, M.J. Watson, G. Webb, J.W. Winfield, Green Chem. 1 (1999) 9.
[17] S. Brunet, B. Boussand, J. Barrault, in: Proc. 11th Int. Cong. Catal., Baltimore (1996), 1996, p. 433.
[18] H. Kim, H.S. Kim, B.G. Lee, H. Lee, S. Kim, J. Chem. Soc. Chem. Comm. (1995) 2383.
[19] D.M.C. Kavanagh, T.A. Ryan, B. Mile, J. Fluorine Chem. 64 (1993) 167.
[20] A. Kohne, E. Kemnitz, J. Fluorine Chem. 75 (1995) 103;
A. Hess, E. Kemnitz, J. Fluorine Chem. 74 (1995) 27.
[21] B. Adamczyk, A. Hess, E. Kemnitz, J. Mater. Chem. 6 (1996) 1731.
[22] F. Seel, Angew. Chem. 76 (1964) 532.
[23] E. Kemnitz, K.-U. Niedersen, J. Catal. 155 (1995) 283.
[24] F.J. Weigert, J. Fluorine Chem. 46 (1990) 375.
[25] N. Ignat'ev, A. Kucherina, P. Sartori, Acta Chem. Scand. 53 (1999) 1110.